Investigation of hurricane Ivan using the coupled ocean–atmosphere–wave–sediment transport (COAWST) model

Joseph B. Zambon · Ruoying He · John C. Warner

Abstract The coupled ocean–atmosphere–wave–sediment transport (COAWST) model is used to hindcast Hurricane Ivan (2004), an extremely intense tropical cyclone (TC) translating through the Gulf of Mexico. Sensitivity experiments with increasing complexity in ocean–atmosphere–wave coupled exchange processes are performed to assess the impacts of coupling on the predictions of the atmosphere, ocean, and wave environments during the occurrence of a TC. Modest improvement in track but significant improvement in intensity are found when using the fully atmosphere–ocean–wave coupled configuration versus uncoupled (e.g., standalone atmosphere, ocean, or wave) model simulations. Surface wave fields generated in the fully coupled configuration also demonstrates good agreement with in situ buoy measurements. Coupled and uncoupled model-simulated sea surface temperature (SST) fields are compared with both in situ and remote observations. Detailed heat budget analysis reveals that the mixed layer temperature cooling in the deep ocean (on the shelf) is caused primarily by advection (equally by advection and diffusion).

Keywords Coupled modeling · Hurricane · Ocean dynamics

J. B. Zambon · R. He (✉)
Department of Marine, Earth and Atmospheric Sciences, North
Carolina State University, Raleigh, NC, USA
e-mail: rhe@ncsu.edu

J. C. Warner
United States Geological Survey, 384 Woods Hole Road, Woods
Hole, MA 02543, USA

1 Introduction

Tropical cyclones (TCs) are a significant cause of displacement, damage, and loss of life to coastal communities. They also represent discrete events causing drastic marine environmental changes. Continued improvement in the prediction of TCs, and their interactions with the atmosphere and ocean environments, contributes to the improvement of information conveyed to emergency managers during landfalling storms. Track forecasts of hurricanes have shown gradual improvements over the years, primarily though improvements to coarse-grid, global models (Marks and Shay 1998; Wang and Wu 2004; Goerss 2006; Bender et al. 2007). Rogers et al. (2006) assert that over the past three decades, and particularly in the last decade, TC forecast track improvements have been attributed to several areas including improved assimilation of satellite and aircraft observations, better representation of the hurricane vortex, and improved representation of tropical physics. However, improvement in TC intensity prediction has been slower (Rogers et al. 2006; Wada et al. 2010). Rogers et al. (2006) demonstrate that 48-h track forecast errors have decreased by nearly 45 % during the 15-year period from 1990 to 2005 (3 % year^{-1}), from approximately 200 to 110 km. During this same period, 48-h strength forecast errors had decreased by only 17 % (1.1 % year^{-1}), from approximately 17 to 14 kt. Chen et al. (2007) attribute this to deficiencies of numerical models in three areas: coarse-grid spacing, poor formulations of the surface and boundary layers, and lack of coupling to a dynamic ocean.

Coarse-grid spacing is a problem being resolved continually through the utilization of faster computational resources. Surface and boundary layer formulations are being improved continually through other process studies. Additional sources of TC intensity forecasting error include poor representation of inner-core dynamical processes (such as eyewall replacement cycles) and poor model initial conditions. Improvements

in the representation of inner-core dynamical processes are a multi-scale problem, as the TC inner-core interacts with the larger-scale environment (Wang and Wu 2004; Davis et al. 2008). Resolving the inner-core of a TC with a grid spacing of less than 4 km has been shown to allow the use of explicit representation of convection, which has resulted in better structure of the TC (Fowle and Roebber 2003; Done et al. 2004). Gopalakrishnan et al. (2012) demonstrates the improvement in TC intensity forecasts by decreasing nested grid spacing from 9 to 3 km, which the current Hurricane Weather Research and Forecasting (HWRF) operational model uses. Intensity also suffers from poor initial conditions and is a result of poor initial TC structure (Gopalakrishnan et al. 2012). Improvement of the initial structure of TCs is currently being examined through the use of data assimilation (Davis et al. 2008).

The last deficiency, lack of coupling to a dynamic ocean, is addressed through several approaches. Coupling TC simulations to three-dimensional ocean and wave models has been demonstrated to be of great importance to the accuracy of intensity forecasting. Accurately resolving the ocean surface, the source of energy upon which TCs rely, is an important consideration for both atmospheric and oceanographic modeling. Price (1981) and Price et al. (1994) have shown that large and/or slow-moving TCs can decrease sea surface temperature (SST) and produce a distinct cooling bias on the right side of hurricanes. Through analysis of observed and data from a coupled atmosphere-wave-ocean model, Wada et al. (2013a) demonstrated a reduction of SST, surface salinity, and partial pressure of surface ocean CO_2 (due to outgassing during TC passage). Wada et al. (2014) featured analysis of three profiling floats in the western Pacific ocean during the 2011 and 2012 typhoon seasons, showing the spatial dependence on SST cooling and its effect on latent heat fluxes and simulated TC intensity. Utilizing a coupled atmosphere–ocean model, Lee and Chen (2014) have demonstrated that the spatial distribution of SST cooling beneath the swirling inflow of a TC results in the formation of a stable boundary layer. The stable boundary layer has the effect of transporting high-energy air near the surface into the eyewall. The introduction of this air into the eyewall then offsets some of the effect SST cooling has on reducing TC intensity. Once SSTs fall below the 26 °C critical value, enthalpy fluxes from the surface are no longer sufficient to sustain TC growth (Leipper and Volgenau 1972). The three-dimensional structure of ocean currents and eddies can further complicate the heat and momentum flux exchange between the ocean and hurricane (Walker et al. 2005; Rogers et al. 2006; Liu et al. 2012). Bender et al. (2007), Shay et al. (2010), and Wada et al. (2010, 2013b, 2014) suggest the importance of initializing coupled models with realistic warm and cold ocean features in the global oceans. Wu et al. (2007) and Ma et al. (2013) use a simplified atmosphere–ocean coupled model and idealized

TC to quantify the effects of ocean eddies on TC intensity. Demonstrated in Oey et al. (2006), Hurricane Wilma forced warm water through the Yucatan Channel into the Gulf of Mexico. After Wilma entered the Gulf of Mexico, the interaction between the warm loop current waters and atmospheric conditions favored rapid intensification. The resulting storm was the strongest hurricane on record in the Atlantic basin. Bender et al. (2007) demonstrates operational Geophysical Fluid Dynamics Laboratory (GFDL) model simulations of the intensity of several TCs in the Atlantic basin were improved by inclusion of a high-resolution, three-dimensional ocean model (in their study, the Princeton Ocean Model; POM) and by improving air-sea momentum flux parameterizations. Wada et al. (2013b) showed that preexisting oceanic conditions had significant effects on simulated intensity and inner-core axisymmetric structure of a simulated typhoon. Yablonsky and Ginis (2009, 2013) demonstrate the importance of a three-dimensional ocean model to resolve SST cooling when simulating a TC translating across the ocean surface at <5 m/s. In addition, Walker et al. (2005) demonstrates biological feedback from Hurricane Ivan. Phytoplankton blooms were found with peak concentrations of 3–4 days after the TCs passage, having important effects on the ecosystem of the central Gulf of Mexico.

The accurate prediction of the wave environment is also of importance in the numerical simulation of a TC (Chen et al. 2007, 2013; Moon et al. 2007; Wada et al. 2010, 2014; Liu et al. 2011, 2012) because it improves prediction of wind speeds, fluxes, and oceanographic mixing. These wave environment feedback mechanisms are crucial to resolving a moving TC in the atmosphere and oceans. Uncoupled wave models have demonstrated good skill, so long as the wind forcing fields are accurate (Fan et al. 2009). However, the variable swirling winds in a TC can be difficult to capture using coarse global meteorological models, which are used by global wave models for surface forcing. In addition, most wind-wave models treat their surface roughness as a scalar quantity (Bao et al. 2000; Doyle 2002). In the TC environment, the winds are highly variable and the surface stress vector is not always aligned with the local wind vector (Chen et al. 2007, 2013), therefore the surface roughness has a directionality component. The coarse-grid spacing of the utilized wind fields and the treatment of surface roughness as a scalar quantity result in poor accuracy from uncoupled wave models.

In this study, we investigate the accuracy of hurricane track and intensity prediction using a series of numerical investigations of increasing complexity by adding more coupling components and physics. Due to its extreme intensity, breadth of data in the atmosphere–ocean-wave environments, and large economic and environmental impacts, Hurricane Ivan was chosen as a case study to employ the recently developed coupled ocean–atmosphere–wave–sediment transport

(COAWST) model (Warner et al. 2010). The COAWST model has been used to study several other coastal storms and their effects on the atmosphere, ocean, and wave environments. These cases include simulations of TCs (Warner et al. 2010), strong Nor'easters (Nelson and He 2012), as well as storms undergoing extra-tropical transition (Olabarrieta et al. 2012).

This paper is organized as follows: Sect. 2 provides a brief description of COAWST modeling system, the methods used to couple the three independent models together, the fields that are exchanged to each individual model, and the five sensitivity experiments we completed to examine the effect of model coupling with increasing complexity in hindcasting Hurricane Ivan. Results and analysis are given in Sect. 3, which demonstrate the improvements in model accuracy through coupling by comparing our five experiments to a combination of in situ and remote observations of the atmosphere, ocean, and wave environments. This is followed by a summary and conclusion of findings in Sect. 4.

2 Modeling system

The COAWST model (Warner et al. 2010) was designed from three state-of-the-art advanced numerical models representing the atmosphere, ocean, and wave environments. Representing the atmosphere is the Weather Research and Forecasting (WRF) version 3.2 model using the Advanced Research WRF (ARW) dynamical core (Skamarock et al. 2005). The WRF model is a nonhydrostatic, quasi-compressible atmospheric model with a number of boundary layer schemes, as well as both explicit and parameterized physics. These options allow simulations to be run on different scales ranging from synoptic to mesoscale.

Representing the ocean environment is the regional ocean modeling system (ROMS) version 3.3. ROMS is a free-surface, terrain-following numerical model that is able to solve the three-dimensional Reynolds-averaged Navier–Stokes equations using hydrostatic and Boussinesq approximations (Shchepetkin and McWilliams 2005; Haidvogel et al. 2008). ROMS can be run using multiple advection schemes, turbulence models, lateral boundary conditions, surface, and bottom boundary layer schemes.

Representing the wave environment is the simulating waves nearshore (SWAN) version 40.81 model. The SWAN model is a spectral wave model that solves the spectral density evolution equation (Booij et al. 1999). SWAN is able to simulate wind-wave generation and propagation in coastal waters. SWAN also includes many physical processes that can be enabled or disabled, including refraction, diffraction, shoaling, and wave-wave interactions. Wave dissipation is available from the physical processes of whitecapping, wave breaking, and bottom friction.

In addition to these numerical models, the community sediment transport model (CSTM) can be coupled to the ocean model and provide the hydrodynamic model with simulated erosion and deposition across many different types and sizes of sediments (Warner et al. 2010). The CSTM is not used in this study; however, a previous study into the transfer of sediments during TCs has been completed with Hurricane Isabel (2003) as a test case (Warner et al. 2010).

These separate models communicate via the model coupling toolkit (MCT; Larson et al. 2004; Jacob et al. 2005; Warner et al. 2008), which is a fully parallelized system that uses the message passing interface (MPI) to exchange model state variables. First, the master program initializes MPI and distributes each model component onto different sets of processors. Each individual model enrolls into MCT and configures its own domain, dynamics, and physics parameters as defined by their respective documentation. Data exchange occurs by MCT at initialization between the models, after which the models integrate by their specified time step to a defined synchronization point. At that instance, data are exchanged between the models. Model integration then continues until the next synchronization point where data are exchanged again. This process is repeated through the end of the models' integrations, during which data are output at the individual models' predetermined intervals. At the end of the models' iterations, the master program finalizes the MCT and MPI and terminates the program.

2.1 Model coupling

The COAWST modeling system allows exchange of prognostic fields between the various components. Variables that are exchanged in the fully coupled experiment are shown in Fig. 1. While the SST is passed from ROMS to WRF, sea surface stresses (τ) and net heat flux are passed from WRF to ROMS. WRF passes winds at 10 m above the sea surface (U_{10}) directly to SWAN, which are used in the computation of significant wave height, average wavelength, and relative peak period to be passed back to WRF.
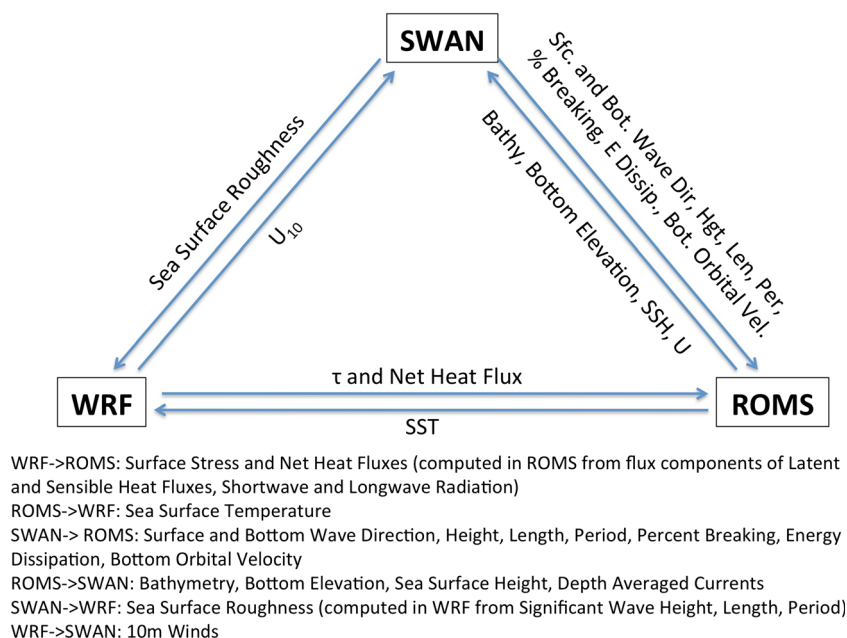
Without wave coupling, surface roughness is computed in WRF based on the Charnock (1955) relation of roughness length to wind stress.

$$z_0 = z_{ch} \frac{u_*^2}{g}$$

where z_0 is the roughness length, z_{ch} the Charnock parameter (a dimensionless value of 0.018), u_* the friction velocity (m/s), and g the acceleration due to gravity (9.81 m/s^2). With the addition of wave coupling, we have a choice of three different parameterizations of sea surface roughness. In our simulations of Hurricane Ivan, the most accurate choice of

Fig. 1 Diagram of three-way coupled model as implemented in the COAWST model

WRF->ROMS: Surface Stress and Net Heat Fluxes (computed in ROMS from flux components of Latent and Sensible Heat Fluxes, Shortwave and Longwave Radiation)
ROMS->WRF: Sea Surface Temperature
SWAN-> ROMS: Surface and Bottom Wave Direction, Height, Length, Period, Percent Breaking, Energy Dissipation, Bottom Orbital Velocity
ROMS->SWAN: Bathymetry, Bottom Elevation, Sea Surface Height, Depth Averaged Currents
SWAN->WRF: Sea Surface Roughness (computed in WRF from Significant Wave Height, Length, Period)
WRF->SWAN: 10m Winds

sea surface roughness was determined by comparison of intensity and wave heights that most closely resembled verification. Based on our comparisons (not shown), we chose to use the Taylor and Yelland (2001) parameterization.

$$\frac{z_0}{H_s} = A_1 \left(\frac{H_s}{L_p}\right)^{B_1}$$

where H_s is the significant wave height (m) and L_p the wave period (s). A_1 and B_1 are constants calculated in Taylor and Yelland (2001) to be 1200 and 4.5 (both are dimensionless values), respectively.

Although the use of a simplified drag formulation coefficient based on the Charnock (1955) relationship has been shown to overestimate drag in high-wind regimes, Moon et al. (2007) demonstrates that there is only a ~10 % increase in strength, and minimal effect on intensity through use of a drag limiter. To investigate this further, we completed additional coupled experiments (not shown) utilizing modified surface bulk drag coefficients according to Donelan et al. (2004) and enthalpy flux coefficients according to Garratt (1992). Through the use of these formulations, our simulations show increased wind speeds but similar intensity and track, in agreement with Moon et al. (2007) and Wada et al. (2013b, 2014). In the modified bulk and enthalpy flux experiments, the SST across the domain was similar to our experiments (within 0.5 °C at all in situ locations) and the stronger wind field resulted in a ~15 % increase in wave heights. These additional experiments demonstrated that the limited drag coefficient approach has an effect and modified enthalpy

fluxes in the high-wind regime should be examined in future study of coupled models in TC environments. However, based on our results demonstrating minimal difference, Hurricane Ivan may not be the most appropriate case for these investigations.

As in SWAN-WRF coupling, sea surface wave parameters passing from SWAN to ROMS include significant wave height, average wavelength, and relative peak period. Surface wave direction, bottom wave period, bottom orbital velocity, percentage of breaking waves, and dissipation energy are also transferred. Sea surface height (SSH) is passed from ROMS to SWAN, as well as east and north currents computed as a vertical distribution of the current profile based on the method of Kirby and Chen (1989). The authors recognize the importance of wave-current interaction in TC forecasting, and we refer interested readers to recent publications from Olabarrieta et al. (2011, 2012) and Kumar et al. (2012). These papers examine wave-current interaction by using the COAWST model for a number of case studies, in addition to ongoing research by the authors for future publication.

The sea surface momentum and heat fluxes for the ocean model can be computed in one of two ways. The original method utilized a bulk flux formulation of Fairall et al. (1996, 2003) and required from WRF 10-m wind vectors ($\overline{U}_{10}$), air temperature (T_{air}), atmospheric pressure (P_{air}), humidity, downward long wave radiation, and net shortwave radiation. The wave (SWAN) model exchanges variables of significant wave height, average wavelength, and relative peak period to ROMS. From these variables, bulk fluxes of surface stress (τ) and heat flux (HF) are computed and used by the ocean model.

However, there are potential problems for use of this configuration in our case. First, their utility in the high-wind

scenarios is subject to further investigation. Second, the combined use of bulk fluxes and in-model parameterizations could result in inconsistent flux calculations between the models. Therefore, we use a second option, which uses the momentum and buoyancy fluxes computed by WRF to directly drive the ocean model. This ensures a consistent forcing between the two models and does not allow for parameterizations to be made in both WRF and ROMS, which could differ significantly, especially in a hurricane environment.

2.2 Experimental design

Hurricane Ivan was an extremely intense Saffir-Simpson category 5 (winds ≥70 m/s) hurricane when it moved through the Caribbean ocean, weakening slightly to a strong Saffir-Simpson category 3–4 (wind speeds 50–70 m/s) hurricane as it moved through the Gulf of Mexico in September 2004, devastating the oil and natural gas industry (Teague et al. 2007). This was a unique hurricane in that it intensified rapidly (maximum wind speed increase of >30 kt within 24 h) at a relatively low latitude (9.7° N), experienced many rapid intensification and decay cycles over the course of its lifetime, and made two landfalls along the Gulf coast (Stewart 2005). This study focuses on its development prior to its first and much more intense landfall, which occurred on 16 September at 0650 UTC, just west of Gulf Shores, Alabama. Hurricane Ivan presents a unique case for model hindcast as the intensification and decay cycles over the course of its lifetime made it very difficult to forecast (Stewart 2005). The challenge of simulating this Gulf of Mexico hurricane transitioning onto the shelf and making landfall while maintaining an extreme intensity was sought in contrast to the comparatively weak hurricanes studied in our previous studies (Warner et al. 2010; Olabarrieta et al. 2012). We use five different coupling configurations of COAWST to investigate model sensitivity to varying complexity in air-sea-wave interaction and feedback (Table 1).

In the first experiment (*Static SST*), the WRF model iterates with an unchanging SST condition based on the Real-Time Global (RTG) SST analysis provided by Gemmill et al. (2007) interpolated to the model initialization time. This represents a case of no ocean feedback to the atmospheric model, and hence no SST cooling signature appears in the ocean model during and after Hurricane Ivan's passage through the Gulf of

Mexico. In the second experiment (*Dynamic SST*), the WRF model executes with the SST input from daily RTG SST analysis (Gemmill et al. 2007), interpolated every 6 h, from initialization to completion. Unlike the static SST experiment, a cooling signature trailing Hurricane Ivan is present in this simulation. The third experiment (*WRF OML*) utilizes a one-dimensional ocean mixed layer (OML) model based on Pollard et al. (1973) and integrated into WRF by Davis et al. (2008). In WRF OML, the OML has been set to a constant 40 m across the domain. The fourth experiment (*2-Way*) enables coupling between WRF and ROMS exclusively. The fifth and final experiment (*3-Way*) demonstrates complete coupling within all of the components of the COAWST model as demonstrated in Fig. 1.

## 2.3 Domain and model configuration

The WRF model domain (encompassing the entire geographic area of Fig. 2) is chosen to incorporate the entire ROMS and SWAN model domains. The WRF domain is significantly larger than the collocated ROMS and SWAN domains. This is designed such that additional grid points are available in order to provide Ivan sufficient model space in order to develop and strengthen after initialization. The WRF model has a horizontal grid spacing of 8 km in the outer domain. ROMS and SWAN grids are collocated, having a horizontal grid spacing of 5 km. As in Warner et al. (2010), grid points had to be interpolated before model initialization for proper data exchange by the MCT. Interpolation weights were utilized in order for the models to exchange information across their spatial domains. The Spherical Coordinate Remapping Interpolation Package (SCRIP) was used to implement a conservative remapping scheme for this purpose (Jones 1999; Warner et al. 2010). The weights are computed using a nearest neighbor bilinear interpolation and then are read in during initialization for use during the models' iteration.

The best initialization time for our model hindcast was determined based on several static SST runs (not shown). From this ensemble, we chose the model run whose track and intensity most closely represented the National Hurricane Center best-track data (hereafter verification) was selected. The simulation that performed best was initialized at 12 UTC on 12 September and terminated at 00 UTC on 17 September, for a total run time of 4.5 days (108 h). This

Table 1 Design of five experiments relating to the level of ocean and wave interaction

Experiment	SST condition	Ocean coupling	Wave coupling
Static SST	RTG SST at initialization, unchanging	None	None
Dynamic SST	RTG SST, updated every 6 h	None	None
WRF OML	Changing based on WRF OML model	1-D Ocean Mixed Layer	None
2-Way	Changing based on ROMS	ROMS model	None
3-Way	Changing based on ROMS	ROMS model	SWAN model

Fig. 2 Comparison of forecast track, five experiments: Static SST (*red*), Dynamic SST (*green*), WRF OML (*cyan*), 2-Way (*blue*), and 3-Way (*magenta*). *Black*, NHC best-track verification. Also shown are the locations of onshore and offshore grid points (S1 and S2) used for analysis in Figs. 7, 8, 9, and 10
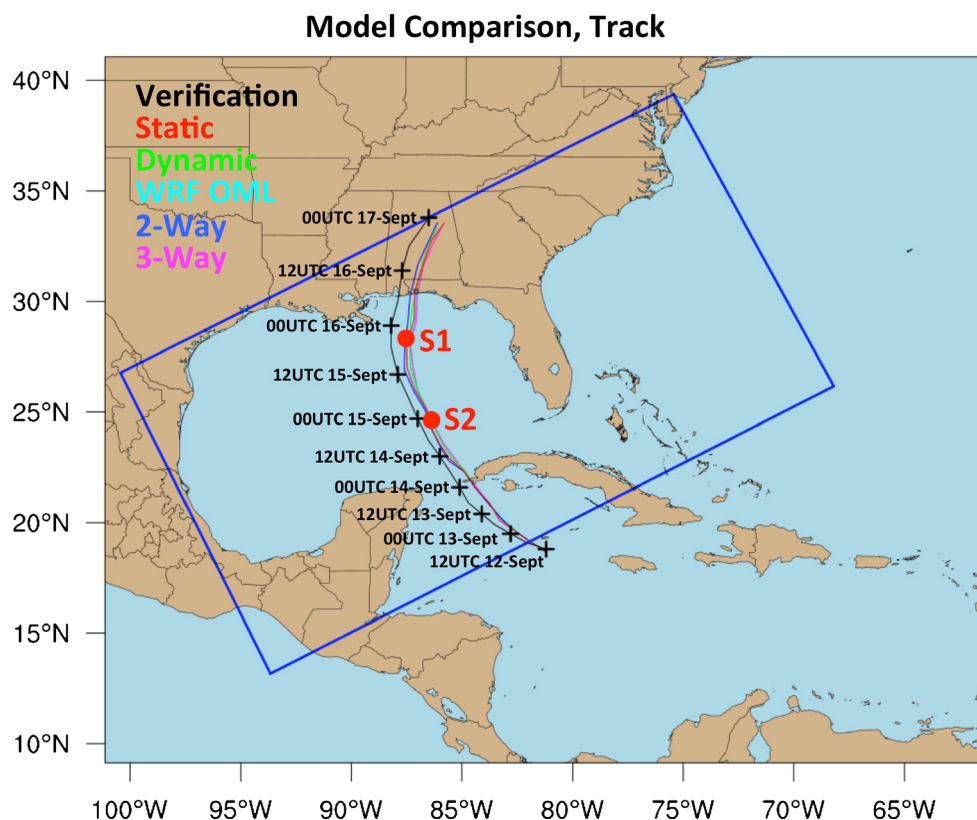
simulation had a slight eastward track error but demonstrated similar translation speed and timing for landfall compared with verification as well as the best comparison to observed intensity. Accurately representing the intensity of strong hurricanes at model initialization has posed a significant hurdle for TC modeling from the atmospheric perspective (Rogers et al. 2006). With the models initialized from a coarse 1° Global Forecasting System (GFS) model solution, the simulated TC had an intensity of 986 hPa, whereas verification demonstrates that Hurricane Ivan had an intensity of 919 hPa at the time. As a result, there was a significant intensity deficit at initialization across all model runs.

Multiple approaches were investigated to alleviate this initial intensity deficit while maintaining an accurate comparison to the 108 h hindcast track. Initialization was attempted from analysis with finer 32 km grids, such as NARR, or using a bogus (simulated vortex) TC modeled on a combination of NHC best-track and H-wind data. In either case, the TC structure and track were not well reproduced. We attribute this issue to the problem discussed in Kurihara et al. (1993, 1995), where the bogus vortex was out-of-balance with the large-scale forcing. To correct this problem, we adopted the GFDL bogus vortex scheme developed by Kurihara et al. (1993, 1995), which divides the large-scale analysis into environmental flow and vortex circulation. The vortex circulation is then divided into axisymmetric (derived from the

axisymmetric perturbation over the prior 12 h) and symmetric components, which are then included in the environmental background flow. Combining the intense and balanced vortex provided by the GFDL product with the large-scale environmental forcing provided by the GFS, we obtain a track that was superior to simulations using GFS alone. There was a more profound change to the initial intensity, greatly reducing the initial gap. The GFS-only simulation initialized TC featured intensity 67 hPa weaker than verification, compared with the blended initialization with intensity 8 hPa stronger than verification. After initialization, the simulation is free to develop and is run without any nudging throughout the 108-h hindcast. The boundary conditions are derived from the GFS solution alone and are updated every 6 h. Completing the hindcast without the added benefit of data assimilation, nudging, etc., was essential to isolating the effects of coupling, one of the primary goals of this study. As a result, our simulations do not provide an exact hindcast of Hurricane Ivan, rather we focus on examining the effect of different complexity of couplings on the hindcast.

To better resolve the TC, the WRF model downscales using a two-way vortex-following moving nested grid. The co-located ROMS/SWAN grids do not feature a nested grid. Halliwell et al. (2011) studied ocean response from Hurricane Ivan utilizing atmospheric forcing from the coupled ocean–atmosphere mesoscale prediction system (COAMPS; Hodur

1997) merged with 10-m vector wind fields (H*WIND; Powell et al. 1998). This study asserts that decreasing horizontal grid spacing below ~10 km in the ocean model grid results in negligible changes to the ocean model result. The WRF outer grid dimensions were 500 (east–west) by 450 (north–south) with 31 vertical levels and 8 km grid spacing. The inner grid is spaced at 2.6 km (a 1-to-3-grid spacing ratio) measuring 301 (east–west) by 301 (north–south) grid points with 31 vertical levels. This inner-nest was required to resolve the TC structure of the eye and eyewall in the atmospheric model (Hill and Lackmann 2009; Gopalakrishnan et al. 2012). In addition, Halliwell et al. (2011) argues that atmospheric forcing that is able to resolve the eye and eyewall of the storm (<10 km horizontal grid resolution in the atmospheric model) is essential in modeling the ocean response. The WRF model time step was defined as 24 s on the outer grid and 8 s on the inner grid. Grid resolved precipitation on both grids was computed using the WRF Single-Moment 6-class microphysics scheme (WSM-6) from Hong and Lim (2006). This first-order microphysics scheme features water vapor, cloud water, cloud ice, rain, snow, and graupel. On the 8-km outer grid, the Kain-Fritsch CP scheme (Kain 2004) was used to parameterize precipitation processes on a sub-grid scale. For the inner grid, the 2.6-km mesh was able to resolve precipitation adequately on a grid scale and no cumulus parameterization was necessary. Longwave and shortwave radiation physics were computed using the Rapid Radiative Transfer Model (RRTM) (Mlawer et al. 1997) and the Dudhia (1989) scheme, respectively, called every 8 min on the outer grid and 2 min on the inner grid. The Eta surface layer scheme (Janjic 1996, 2002) based on similarity theory (Monin and Obukhov 1954) physics option was used along with the Noah land surface model (Chen and Dudhia 2001) for both grids. The Mellor-Yamada-Janjic turbulent kinetic energy planetary boundary layer (PBL) model (Mellor and Yamada 1982; Janjic 1990, 1996) was called every time step on both WRF domains.

The ROMS/SWAN domain (bordered by the blue box in Fig. 2) was on a rotated rectangular grid with a horizontal grid spacing of 5 km. The ROMS model utilized 36 stretched terrain-following vertical levels with a finer vertical grid near the surface and bottom in order to better resolve the ocean boundary layers (Hyun and He 2010). A 25-s baroclinic time step was used. Open boundaries along the eastern and southern portions of the domain are specified with values from the 1/12°, global HYbrid Coordinate Ocean Model with Naval Research Lab (NRL) Coupled Ocean Data Assimilation (HYCOM/NCODA) solutions, which assimilate satellite SSH and SST as well as in situ observations from expendable bathythermographs (XBTs), ship board conductivity temperature depth (CTD), and ARGO floats (Chassignet et al. 2006). We followed the scheme of Marchesiello et al. (2001), whereby Orlanski-type radiation conditions were used in conjunction with relaxation (with timescale of 0.5 days on inflow

and 10 days on outflow) to pass HYCOM/NCODA tracer (salinity and temperature) and three-dimensional velocity fields to ROMS. For the free-surface and depth-averaged velocity boundary conditions, we adopted the method of Flather (1976) with the external values defined by HYCOM/NCODA, updated every day. In our ROMS setup, we used Mellor and Yamada (1982) to compute vertical turbulent mixing, as well as the quadratic drag formulation for the bottom friction specification.

The SWAN model was solved on the same grid as the ROMS model. Boundary conditions were derived from solutions of the global WaveWatch 3 (WW3) model (available at http://polar.ncep.noaa.gov/waves/index2.shtml) and are updated every 3 h. In our SWAN setup, directional space was utilized with 36 directional bins and 24 frequency bins of 1 s width between 1 and 25 s. Nonlinear quadruplet wave interactions were activated in the model. Wave bottom dissipation was parameterized using the Madsen et al. (1988) formulation, with an equivalent roughness length scale of 0.05 m. The depth-induced breaking constant, e.g., the wave height to water depth ratio for breaking waves, was set to 0.73. Wind-wave growth was generated using the Komen formulation (Komen et al. 1984). A backward-in-space, backward-in-time advection scheme was used for iteration.

3 Results and analysis

3.1 Atmosphere

The simulated storm tracks from each of the five experiments, along with verification, are compared in Fig. 2. Variations in Hurricane Ivan's track with coupling scheme are relatively minor and consistent with the earlier assertion that track is largely dependent on large-scale atmospheric circulation processes and less influenced by ocean–atmosphere interaction on the time and spatial scales of the models. Position error (Fig. 3, top panel) is computed as the difference between NHC best-track locations of the storm center at 12-h intervals and the model location of the minimum sea level pressure. The run that best represented the TC track consistently was the 2-Way experiment. However, the difference between the track error among the experiments is quite small throughout the forecast: within 20 km through the first 60 h and within 40 km after that.

As far as simulating Hurricane Ivan's intensity (Fig. 4), strong differences between modeled TCs begin to show almost immediately after the TC enters the ROMS/SWAN domain (approximately 8 h after initialization). The difference in modeled intensity against verification is shown in Fig. 3 (bottom panel) where positive (negative) values denote overintensification (underintensification). While the introduction of the ocean model resulted in underestimation of TC intensification, the magnitude of error of intensity is reduced

Fig. 3 Simulated TC position (km) and intensity (hPa) errors from initialization (12 UTC on 12 September 2004) through termination (00 UTC on 17 September 2004), five experiments: Static SST (*red*), Dynamic SST (*green*), WRF OML (*cyan*), 2-Way (*blue*), and 3-Way (*magenta*)
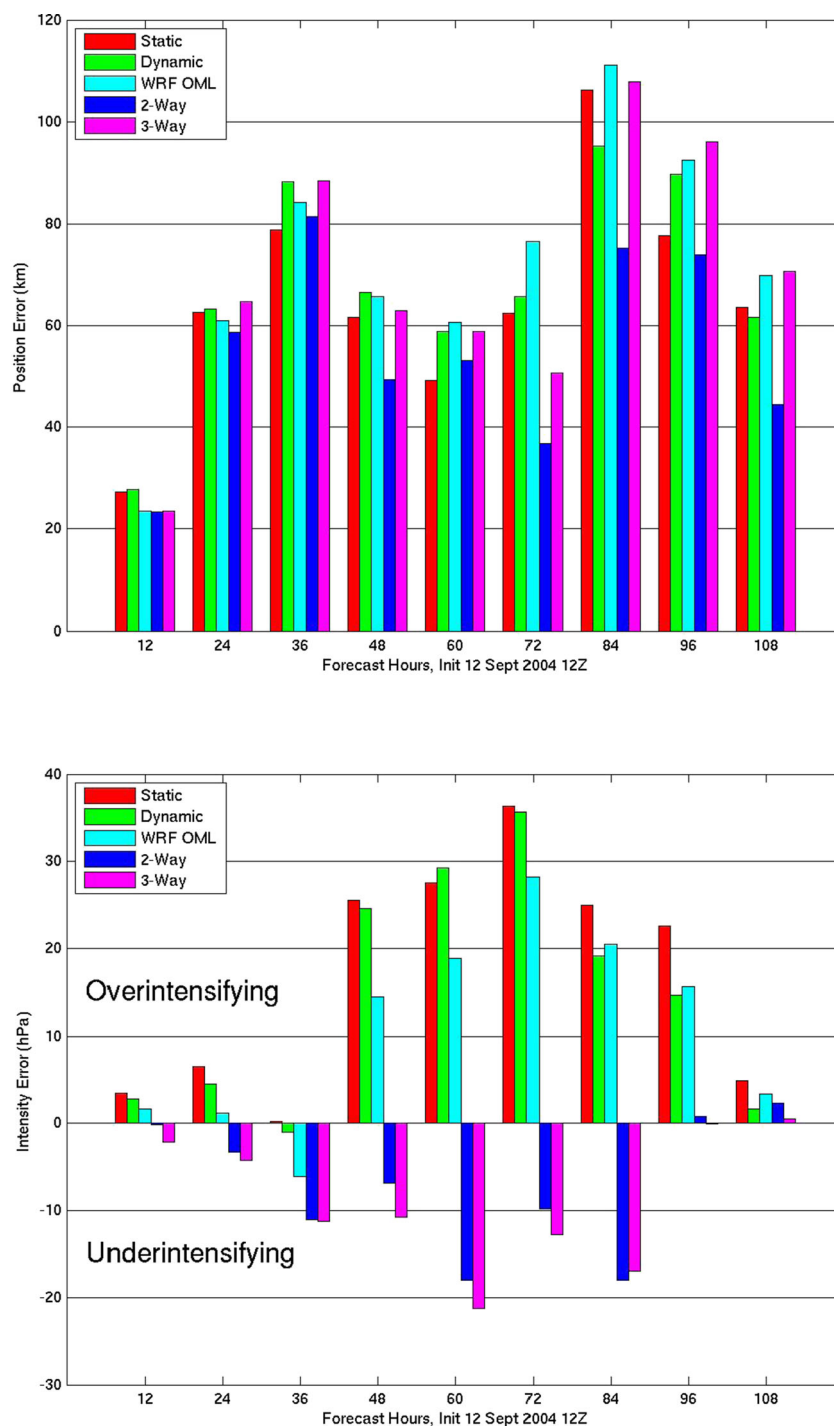

in both coupled cases compared with the three uncoupled cases. In addition, the root-mean-square error (RMSE) and correlation coefficient (*r*) of TC intensity (Table 2) demonstrates that the two coupled experiments were more accurate in representing Ivan's intensity than the uncoupled experiments.

As shown in Fig. 4, the temporal evolution and trends present in observed intensity are not present in the uncoupled

runs. This lack of trend is found even when including ocean feedback through use of a hindcast SST condition (Dynamic SST) or integrating a one-dimensional OML model (WRF OML). The coupled models most accurately resolved the trends of TC intensity throughout the run, especially when Ivan experienced rapid weakening as it entered the Gulf of Mexico. Given that the storm evolution was better predicted using a coupled model, the complexity of the ocean condition,

Fig. 4 Simulated TC intensity from initialization (12 UTC on 12 September 2004) through termination (00 UTC on 17 September 2004), five experiments: Static SST (*red*), Dynamic SST (*green*), WRF OML (*cyan*), 2-Way (*blue*), and 3-Way (*magenta*). *Black*, NHC best-track verification
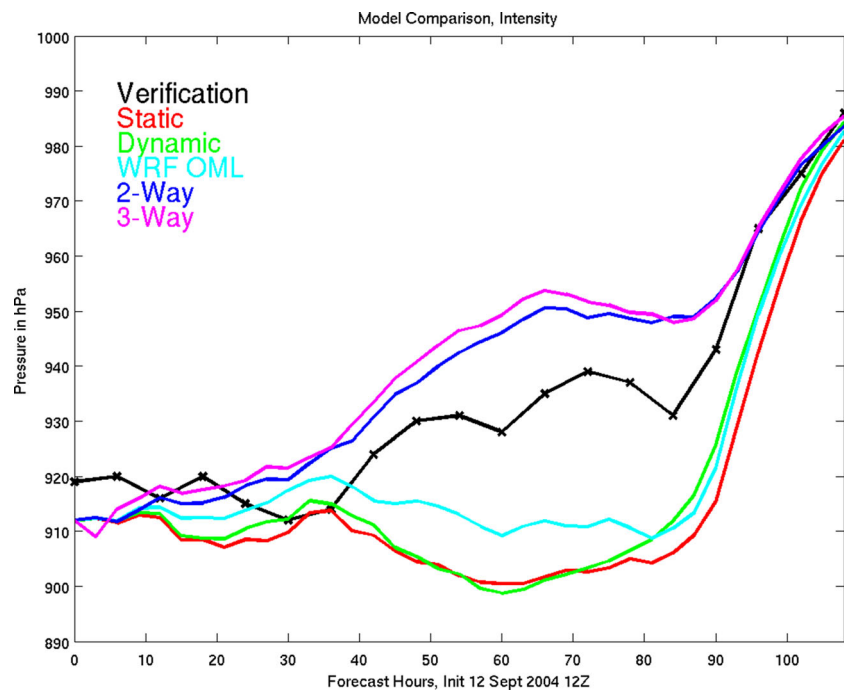
specifically the spatial distribution of SST within the Gulf of Mexico, would need to be examined before and after Ivan's passage.

3.2 SST analysis

The spatial variation of modeled SST in the Gulf of Mexico is shown in Fig. 5 for the WRF-only Dynamic SST and WRF OML cases, the COAWST 2-Way and 3-Way coupled experiments, and the Geostationary Operational Environment Satellites (GOES) SST data. The GOES SST data were obtained from the JPL Physical Oceanography Distributed Active Archive Center (PODAAC). The Static SST case is intentionally left out, as it is represented by the pre-storm condition of the Dynamic SST case throughout the model run.

Due to cloud cover being associated with hurricane, GOES SST data were obscured over a large swath of the West Florida Shelf immediately before model initialization time. In order to provide an initial analysis, GOES SST was averaged over 3 days before model initialization (9 September 12 UTC

through 12 September 12 UTC), hereafter referred to as the pre-storm SST. Likewise, cloud cover required averaging of the daily GOES SST observations from 17 September 00 UTC through 18 September 00 UTC (hereafter, post-storm SST). To be consistent, a similar averaging procedure was done for model-simulated SST fields for comparison.

As previously mentioned, a number of factors result in fluctuations of hurricane intensity. These include but are not limited to SST below the storm, eyewall replacement cycles, wind shear, formation of a stable boundary layer in the SST cold wake, and synoptic-scale atmospheric forcing (Fowle and Roebber 2003; Done et al. 2004; Wang and Wu 2004; Rogers et al. 2006; Chen et al. 2007; Davis et al. 2008; Lee and Chen 2012, 2014). For the purposes of our experiments, the only difference between the simulations is the variation in ocean SST and sea surface roughness to the atmospheric model. Therefore, everything else being equal, the atmospheric model resolves TCs with vastly different intensities based on differences in SST and sea surface roughness. We examine these different intensities using the SST as the mechanism driving the differences, and we offer a chronological explanation of the intensity variation using SST as the primary indicator of storm intensity for our experiments.

At model initialization, 12 UTC on 12 September, the location of Ivan in a region of 30 °C SST south of Cuba helped the storm to intensify to 919 hPa. From this point, until F36 (00 UTC on 14 September) relatively constant temperatures along the storm track resulted in minimal changes to Ivan's intensity. As Ivan crossed the Yucatan Strait and into the Gulf of Mexico, cool SSTs are coincident with a sharp reduction of intensity. This signal is apparent in observations, from F36

Table 2 Intensity comparisons against verification for five experiments over 108 h hindcast. Includes root-mean-square error (RMSE), and correlation coefficient (r) for Intensity (hPa)

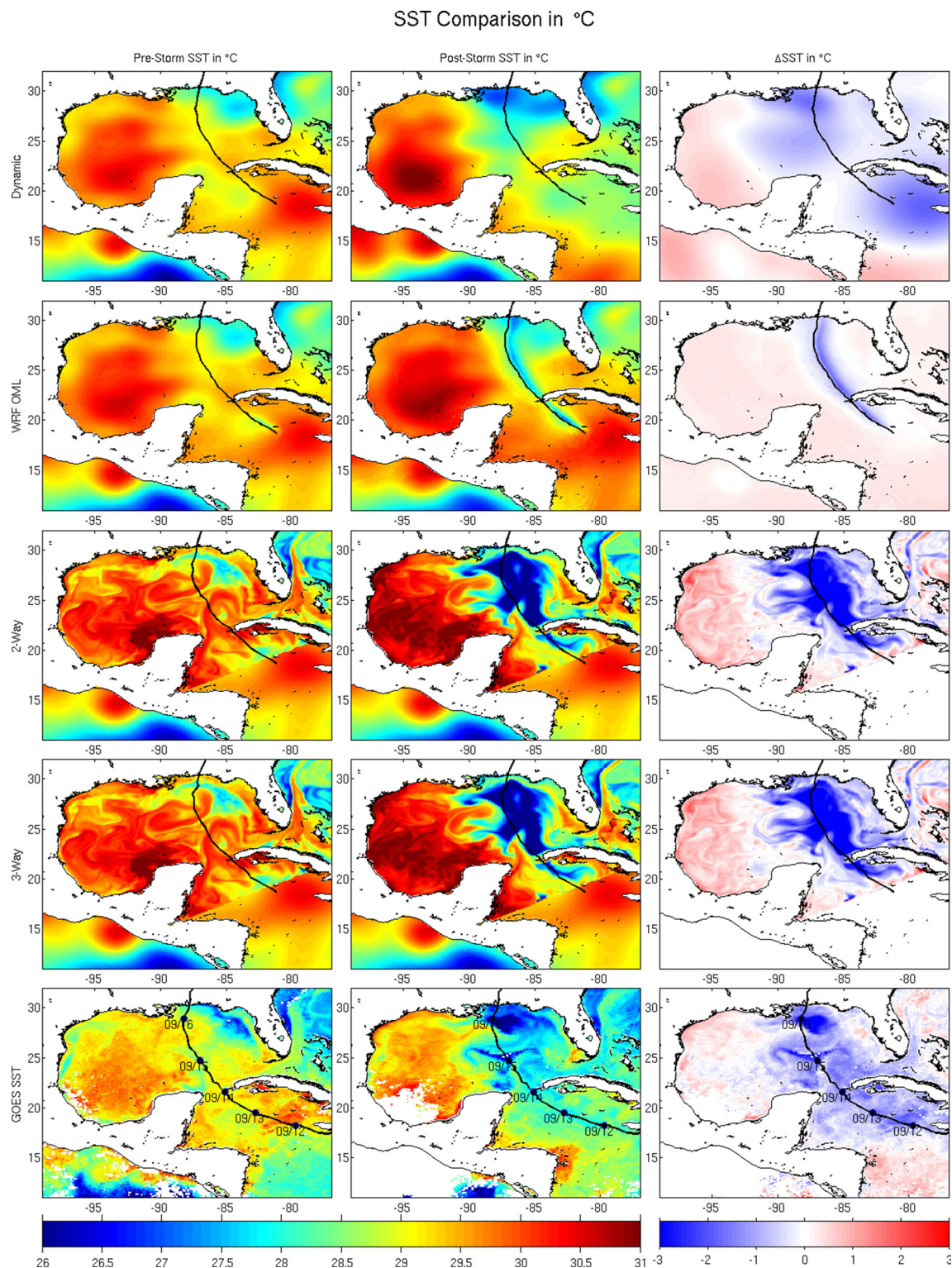|	Intensity	
	RMSE	r
Static SST	20.82	0.85
Dynamic SST	19.16	0.86
WRF OML	15.20	0.88
2-Way	9.66	0.94
3-Way	10.95	0.92

SST Comparison in °C

Fig. 5 Coupled SST comparisons for various experimental cases: Dynamic SST based on the Gemmill et al. (2007) SST analysis (*first row*). WRF OML based on Pollard et al. (1973) and integrated into WRF by Davis et al. (2008); *second row*). Two-Way, atmosphere–ocean, model coupling (*third row*). Three-Way, atmosphere–ocean-wave, model coupling (*fourth row*). GOES SST data obtained from the JPL Physical Oceanography Distributed Active Archive Center (PODAAC; *fifth row*). Pre-storm averaged model SST (*top 4 rows, left column*). Post-storm averaged model SST (*top 4 rows, middle column*). Pre-storm averaged GOES SST (*bottom row, left column*). Post-storm averaged GOES SST (*bottom row, middle column*). Change in SST (*right column*)

through F48 (Fig. 4). From F48 through F60, there is some very slight intensification, as Ivan is passing a region where pre-storm SSTs are shown to be above 29 °C. The crossing of Ivan over cold water on 15 September corresponds to the 13-hPa weakening from F60 to F72. Just prior to landfall, Ivan passed over warmer water on 16 September, concurrent with an observed 10 hPa intensification from F72 to F84 (Fig. 4), followed by a rapid weakening with landfall.

None of the uncoupled runs (Static SST, Dynamic SST, and WRF OML) in Fig. 4 reflect any of these fluctuations with spatial variation of SST. The coupled model runs do accurately demonstrate this weakening, with a distinct decrease in intensity at F36–F72 in the 2- and 3-Way coupled cases. This diminished intensity coincides with the TC cooling the waters in the Gulf of Mexico as resolved by ROMS. In the uncoupled cases, significant decreases in intensity are absent until landfall. Even with the inclusion of a one-dimensional OML model, the WRF OML case demonstrated increasing intensity from F36 until landfall, against the trend shown in observations. As a result, the coupling of a fully three-dimensional ocean model to WRF is necessary to correctly resolve the source of energy on which TCs intensify or weaken.

Of concern in the coupled model cases is the comparison of the modeled pre-storm SST to the GOES SST, which shows a 0.5–1.5 °C warm bias in the model (Fig. 5). In Fig. 6, in situ buoy data at five locations are used to compare the coupled (2-Way and 3-Way) SST, satellite-derived SST, and in situ SST. At each of the five locations along Ivan's track in the Gulf of Mexico, the in situ data show the satellite SST data tend toward a cold bias in the pre-storm environment. As a result, while the satellite-derived SSTs of the pre-storm environment in Fig. 6 are colder than model results, the in situ measurements indicate this discrepancy may be a result of GOES SST cold bias.

When comparing the change in SST during Ivan's passage, the spatial distribution of SST change (ΔSST) demonstrated in Fig. 5 is similar between the coupled models, GOES SST, as well as previous studies (Walker et al. 2005; Prasad and Hogan 2007). The uncoupled experiments, including the WRF OML case, do not demonstrate ocean eddies and other complex circulation structures that can only be resolved with a coupled model (Halliwell et al. 2011; Jaimes et al. 2011). Both coupled models demonstrate larger magnitude and breadth of deep-ocean cooling along the right side of the track when compared with the satellite-derived ΔSST. Buoy time series (Fig. 6), which shows that model-derived SSTs on the right side of the track (e.g., Station 42003) are cooler than the in situ measurements, also indicating an overestimate in cooling in the model on this side of the storm track. Station 42039, also located on the right side of the storm track, demonstrates a model cold bias on the continental shelf, although much less severe. This greater cooling of SSTs partly explains the underintensification of the TC in the coupled cases (in

agreement with Lee and Chen 2012), and it is more significant in the 3-Way coupled case, compared with the 2-Way coupled case. This effect is also demonstrated in Wada et al. (2010) and is largely due to the enhanced mixing of the ocean provided by effects introduced by wave modeling.

The spatial extent of the SST cooling demonstrates that the right-side cooling bias is enhanced in the 3-Way coupled simulation when compared with the 2-Way simulation (Fig. 5). This difference is confirmed in the in situ time series (Fig. 6). To investigate this, we examined the surface stress (not shown) as the intensity, strength, and surface roughness formulation of the experiments differ. For the 3-Way experiment, the surface stress was higher (lower) on the right (left) side of the TC track. The SST was lower (higher) on the right (left) side of the track, partly owing to this difference in surface stress. For this study, this was a minor effect as the difference in SST cooling was within 0.25 °C in all in situ time series comparisons and was within 1 °C throughout the domain. While negligible for our case, further examination of the inclusion of wave effects on SST in this complex ocean–atmosphere–wave coupled environment is subject to further study.

3.3 Mixed layer prognostic variable analysis

In order to investigate the SST difference between stations on the continental shelf and in the deep ocean, we conduct a time series analysis similar to Prasad and Hogan (2007) of the sea surface stress (τ) and heat flux, mixed layer (ML) temperature, and three-dimensional currents were examined at two locations along with the modeled track (S1 and S2 shown in Fig. 2). S1 was chosen to represent a point on the continental shelf, and S2 was selected to represent the temperature and heat budget of the deep ocean. As the 2- and 3-Way SST results are similar (Figs. 5 and 6), only analysis for the 2-Way case is provided to simplify the analysis to specifically demonstrate the impacts of ocean dynamics, without the inclusion of wave effects.

Analysis at point S1 (Fig. 7) demonstrates the response of the OML on the continental shelf to Ivan's passage. Surface wind stress (τ) gradually builds up, peaks, changes direction, and rapidly falls off as Ivan moved over the location. The net heat flux (positive indicating flux into the ocean) is dominated by short wave solar radiation demonstrating a clear diurnal cycle throughout the model run. When Ivan tracked through this location on 16 September, the ocean released heat to the TC (atmosphere). This, along with limited solar radiation due to cloud cover, produced a negative net heat flux. The stronger surface wind stress enhanced mixing, resulting in a cooler surface temperature and eroded thermocline. Positive U represents eastward motion, positive V represents northward motion, and positive W represents motion toward the ocean bottom. The U and V currents clearly demonstrate an inertial
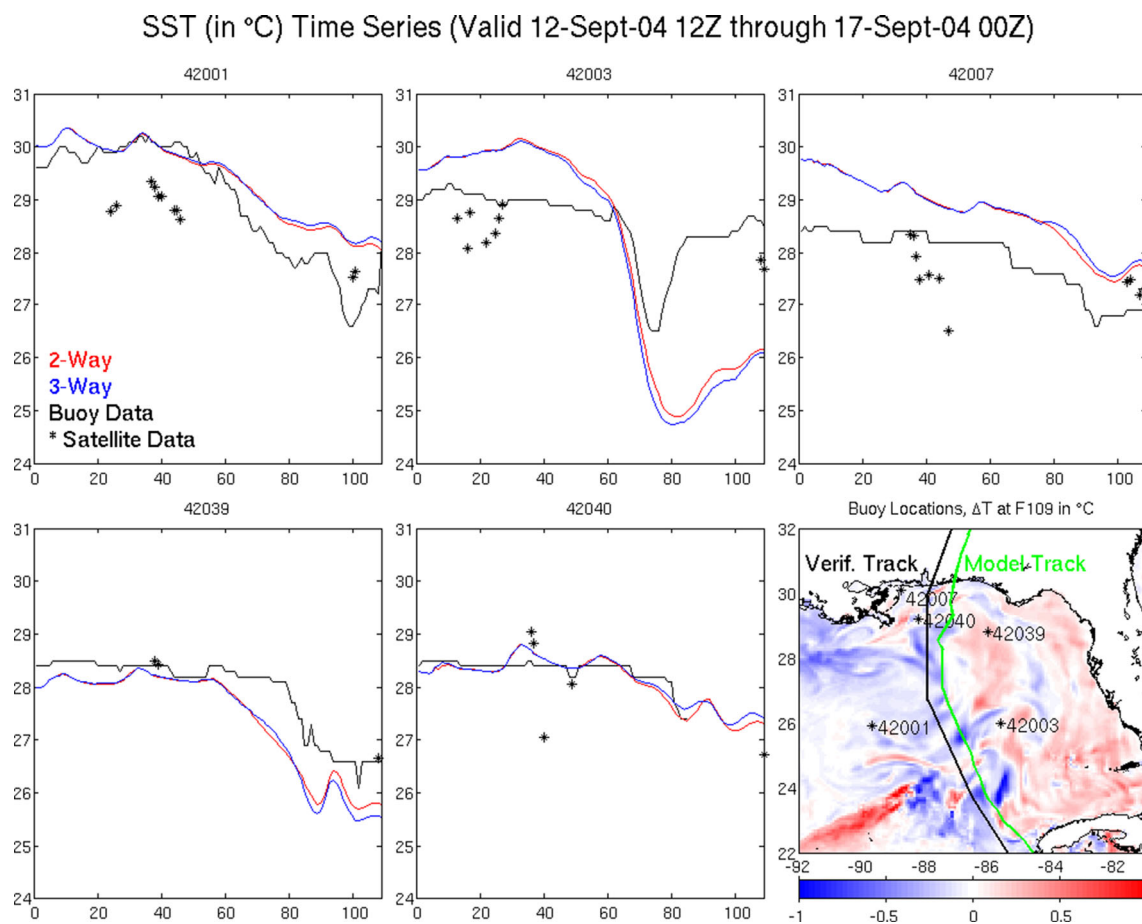
Fig. 6 SST time series at five buoys situated inside of the Gulf of Mexico, showing 2-Way (*red line*) and 3-Way (*blue line*) SST, satellite-derived SST (*black asterisks*), and in situ SST (*black line*). Spatial difference in SST between 2- and 3-Way cases at conclusion of model run, along with location of buoys and 3-Way simulated TC track (*bottom right panel*)

oscillation after the TC's passage with a period of approximately 1 day.

At the offshore point S2 (Fig. 8), the temperature distribution with depth is very different than for S1. The thicker ML prevents complete erosion, and the thermocline remains established well below the surface. While temperatures near the surface drop significantly as Ivan passes (also demonstrated in Figs. 5 and 6), they remain well above the 26 °C critical value for TC development (Leipper and Volgenau 1972). As at point S1, a strong negative heat flux exists during the storm passage and the ocean velocity fields (*U*, *V*, and *W*) demonstrate an inertial oscillation after the TC passes.

3.4 Mixed layer heat budget analysis

The ML heat budget can be diagnosed by piecing out the relative contribution of each term in the heat budget equation.

$$\frac{\partial T}{\partial t} = -u\frac{\partial T}{\partial x} - v\frac{\partial T}{\partial y} - w\frac{\partial T}{\partial z} + \frac{\partial}{\partial z}\left(k\frac{\partial T}{\partial z}\right)$$

where $-u\frac{\partial T}{\partial x} - v\frac{\partial T}{\partial y}$ is the horizontal advection, $-w\frac{\partial T}{\partial z}$ is the vertical advection, $-u\frac{\partial T}{\partial x} - v\frac{\partial T}{\partial y} - w\frac{\partial T}{\partial z}$ represents total advection, $\frac{\partial}{\partial z}\left(k\frac{\partial T}{\partial z}\right)$ is vertical diffusion, and $\frac{\partial T}{\partial t}$ the local rate of change in temperature measured in degrees Celsius per day. We neglected horizontal diffusion terms because they are orders of magnitude smaller. These terms are calculated as diagnostic variables, derived directly from output of the ocean model.

At the onshore point S1, before the storm's passage, the weak diurnal oscillations in *U*, *V*, and *W* are found in both the horizontal and vertical advection terms of Fig. 9. In the pre-storm environment (12 September 12 UTC through 15 September 00 UTC), the horizontal advection terms and vertical advection terms oscillate but are out of phase and therefore cancel each other out (shown in the total advection term). Immediately prior to the eyewall passage (15 September 00 UTC through 15 UTC), cooling due to upwelling is negated by horizontal advection at the surface. Below 30 m, there is a warming trend due to horizontal advection, which creates a positive total advection term in this part of the ML. As the TC passes through, there is strong cooling due to horizontal

Fig. 7 Ocean model (2-Way) analysis at point S1 on Fig. 2 from initialization (12 UTC on 12 September 2004) through termination (00 UTC on 17 September 2004). Wind stress (τ) in newtons per square meter (*first panel*), heat flux (HF) in watts per square meter (*second panel*), temperature from surface through 100 m depth in degrees Celsius (*third panel*), *U* velocity from surface through 100 m depth in meters per second (*fourth panel*), *V* velocity from surface through 100 m depth in meters per second (*fifth panel*), and *W* velocity from surface through 100 m depth in meters per second (*bottom panel*)
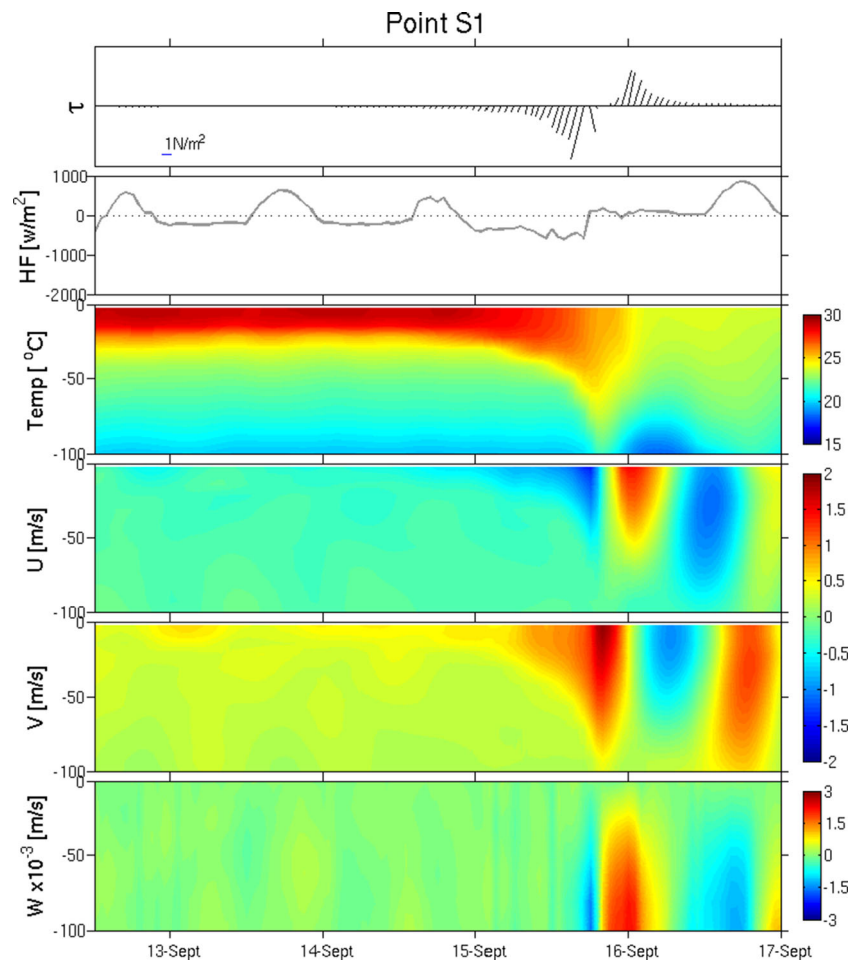
advection through the entire water column that is negated in the upper 40 m by downwelling. Afterwards, the wind stress is reduced with TC passage, although horizontal advection begins to warm the entire water column, the upper 60 m is negated by cooling from vertical advection.

The contribution of the vertical diffusion term to the heat budget is small until the arrival of strong surface wind stresses (15 September 00 UTC to 15 UTC). The temperature diffusion is strongly negative at the surface and positive below 40 m. Throughout the storm event, the total heat flux becomes very negative at the surface due to losses to the atmosphere. As a result of the combination of these factors, just before the eyewall passes, the ML is deepened and the surface temperature is reduced.

As the eyewall passes and the wind shifts (15 September 15 UTC through 16 September 00 UTC), horizontal and vertical advection near the surface are both extremely strong but, as in the pre-storm period, opposite in phase, canceling each other out above 20 m. There is also strong heat loss to the atmosphere through diffusive fluxes near the surface. Below 20 m, intense upwelling causes the advection term to be strongly negative. As a result, there is great heat loss throughout the entire water column as the TC passes, cooling the ML and

eroding the thermocline. The contributions of heat loss during this period are approximately evenly split between advection and diffusion. As the storm winds subside (00 UTC on 16 September), there is an inertial oscillation of *U*, *V*, and *W* causing the ML to be alternately cooled and warmed with a period of approximately 1 day. Time series (Fig. 9, bottom panel) of each heat budget term averaged over the mixed layer depth (MLD; roughly upper 100 m) $\frac{\int_{MLD} f(z)\,dz}{MLD}$ show that contributions from ocean entrainment and diffusion are equally responsible for the cooling trend of the continental shelf ocean during the passage of the storm.

At the deep ocean point S2 (Fig. 10), ocean advection plays a larger role than diffusion in changing the thermodynamic profile of the ML throughout the storm event. Prior to Ivan's passage, the horizontal and vertical advection terms are roughly equivalent in the upper 20 m of the profile. However, as Ivan treks to this point, there is significant transport of warm water below the surface. This is a signature of Ivan pushing warm water northward to this location, an effect similar to what has been shown in Oey et al. (2006) with Hurricane Wilma introducing warm water to the loop current.

Fig. 8 Ocean model (2-Way) analysis at point S2 in Fig. 2 from initialization (12 UTC on September 12, 2004) through termination (00 UTC on September 17, 2004). Wind stress (τ) in newtons per square meter (*first panel*), heat flux (HF) in watts per square meter (*second panel*), temperature from surface through 100 m depth in degrees Celsius (*third panel*), *U* velocity from surface through 100 m depth in meters per second (*fourth panel*), *V* velocity from surface through 100 m depth in meters per second (*fifth panel*), and *W* velocity from surface through 100 m depth in meters per second (*bottom panel*)
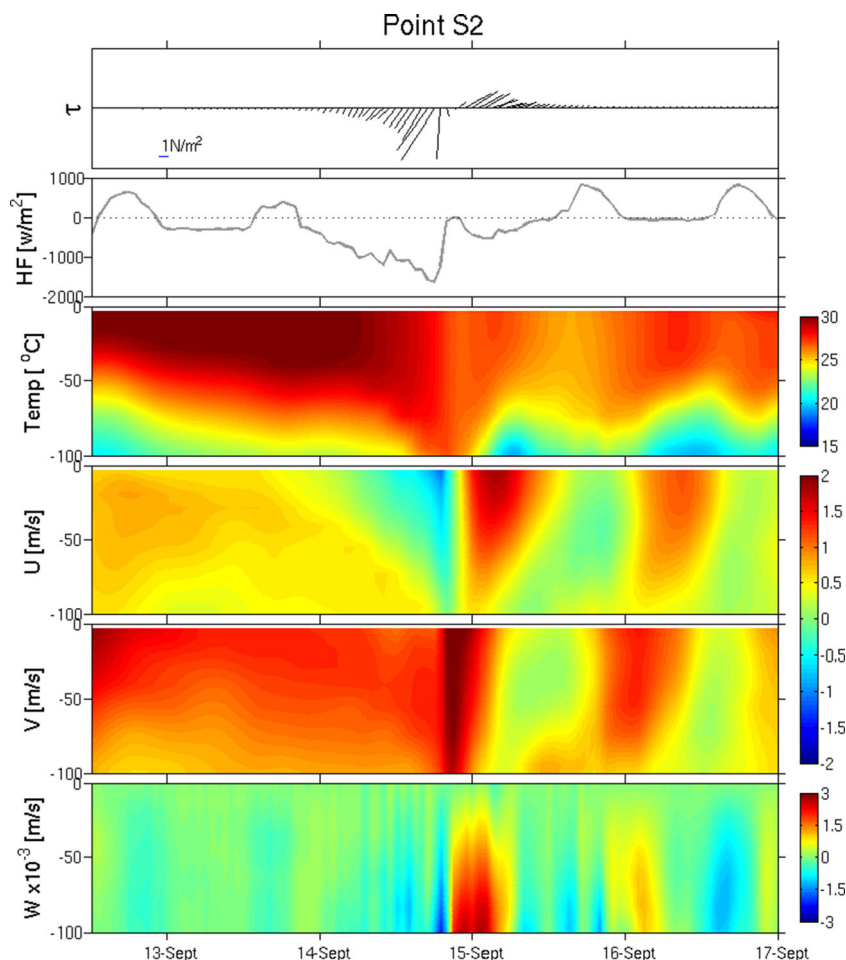
There is a strong upwelling signature before the passage of the TC eye (around 12 UTC on 14 September). This upwelling is weakly relaxed by horizontal advection in the upper 50 m but strongly negated in the lower 50 m. Cooling by vertical advection in the upper 50 m, along with warming by horizontal advection in the lower 50 m, cause the ML to initially deepen before the wind shift at 21 UTC on 14 September. After the wind shift, the contributions of vertical and horizontal advection reverse and there is brief warming near the surface and cooling below. The thermocline is then almost completely eroded through to the surface. As with the nearshore point, after the winds diminish, there is an inertial oscillation of *U*, *V*, and *W* with a period of approximately 1 day causing the ML to fluctuate between warming and cooling.

Diffusion plays a much less significant role at this offshore location, demonstrating only a modest contribution from negative diffusion at the surface and warming below as the eyewall passes at 21 UTC on 14 September. In contrast to the shallow water point, the vertically averaged heat transfer time series demonstrates that entrainment of cooler water

accounts for a much larger proportion of heat transfer in the deep ocean, which is consistent with Price (1981).

3.5 Wave analysis

To examine the results from the wave model, we compared significant wave heights available from the National Data Buoy Center (NDBC) during this storm event. The same five buoys from the earlier SST comparison were used for spatial and temporal comparison of the waves produced with the 3-Way experiment. The results, shown in Fig. 11, demonstrate overall good agreement with in situ observations.

Despite the eastward deviation in track, modeled results at most of the offshore buoys compared well with observations as demonstrated by the RMSE and correlation coefficients. The worst performing comparison, at buoy 42007, is in close proximity to the shoreline (having a model-resolved depth of 12 m). The comparison suffers due to complicated shorelines and bathymetry, which are not well resolved by the 5-km horizontal grid spacing of the model. On the continental shelf, we examine results from buoys 42040 and 42039.
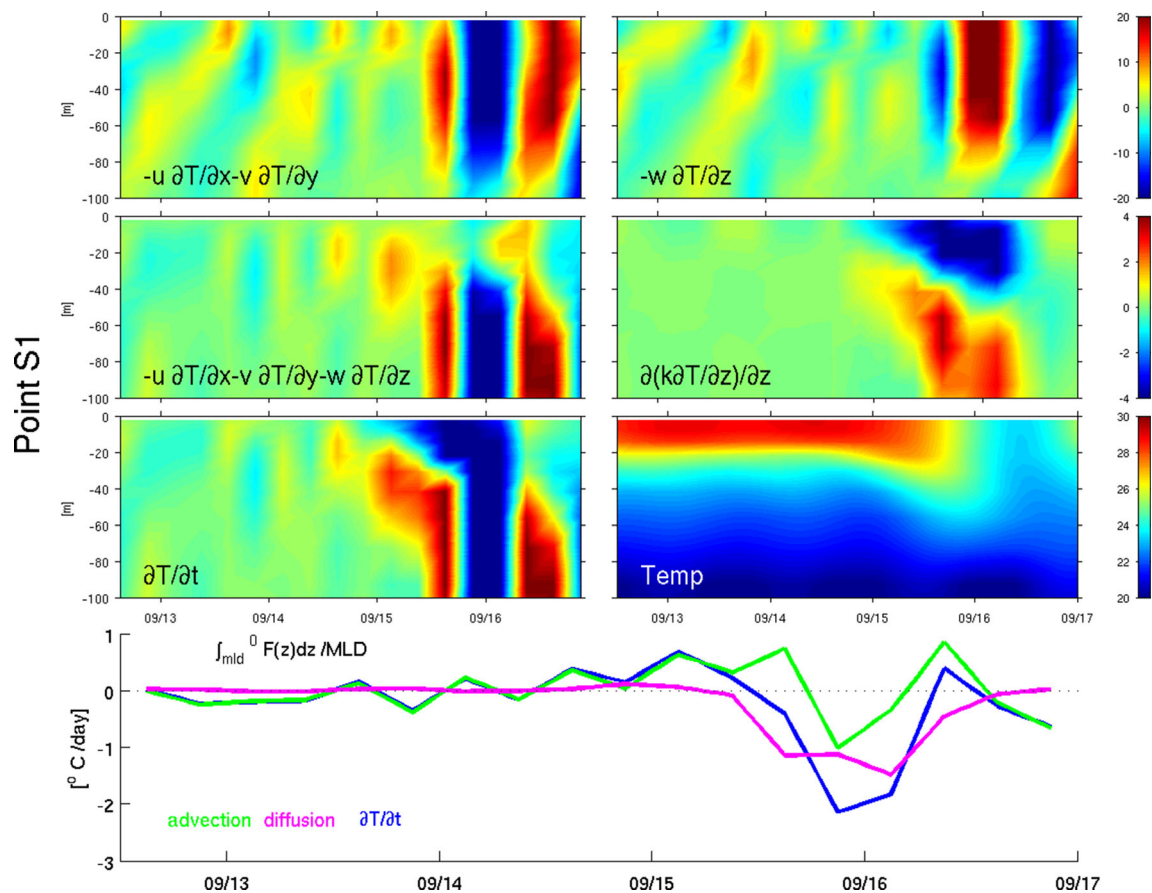
Fig. 9 Ocean model (2-Way) analysis of heat budget at point S1 in Fig. 2 from initialization (12 UTC on 12 September 2004) through termination (00 UTC on 17 September 2004). Horizontal advection term in degrees Celsius per day (*upper left*), vertical advection term in degrees Celsius per day (*upper right*), total advection term in degrees Celsius per day (*middle left*), vertical diffusion term in degrees Celsius per day (*middle right*), total local rate of change term in degrees Celsius per day (*lower left*), temperature in degrees Celsius (*lower right*), and comparison of contributions of advection and diffusion to local change in temperature integrated through 100 m (*bottom panel*)

At 42039, the solution suffered somewhat as the wave heights reduced more rapidly with Ivan's passage in the model than in the observations. This resulted in the model underestimating the waves after the peak at approximately F085, which increased the RMSE. At 42040, the temporal comparison is very good, with both the model and observations demonstrating increasing wave heights at approximately the same time. With the eastward deviation in track, the model did not resolve the peak of significant wave heights to the extreme level that was observed. The greater than 15 m waves were so intense that they tore the buoy from its mooring (Teague et al. 2007), and wave heights were no longer reported after 00 UTC on 16 September.

Off the shelf, two buoys 42001 and 42003 were considered. They are roughly equidistant from the observed and modeled track in the Gulf of Mexico. At 42001, off to the west of the storm track, the peak of the simulated waves is delayed compared with the observations. In addition, the eastward deviation of the modeled TC causes the significant wave height of the simulated waves to be slightly less than observed. At 42003, the eastward deviation in modeled track causes the waves to build up more quickly than observed. However, the peak magnitude of the simulated waves is very close to what was observed. A RMSE of 0.93 and correlation coefficient of 0.97 is demonstrated at this location.

4 Summary and conclusions

Large-scale, global models representing the atmosphere have gradually improved track prediction of TCs over the last several years (Goerss 2006). However, prediction of TC intensity still leaves much to be desired, leading to errors in surface forcing for ocean and wave models. Deficiencies in TC prediction are attributed to, among other causes, lack of coupling to an ocean model (Chen et al. 2007). The newly developed COAWST
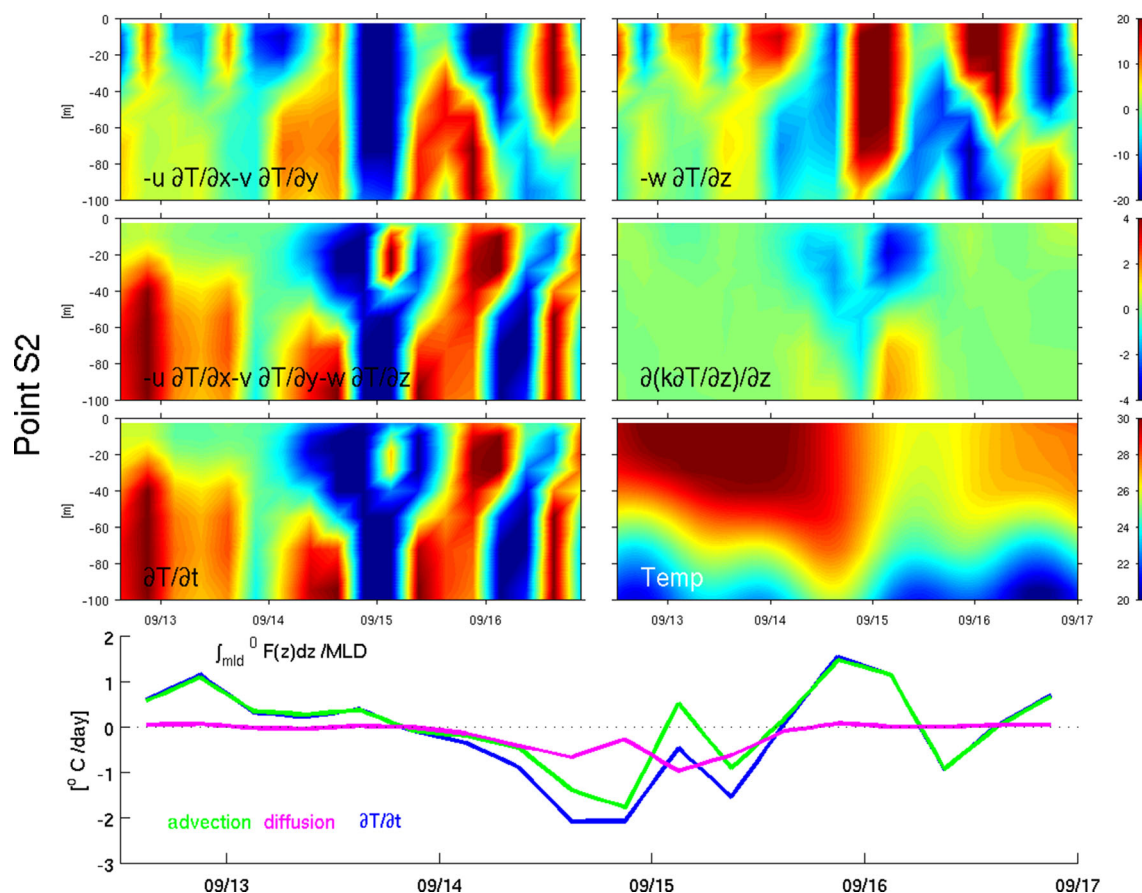
Fig. 10 Ocean model (2-Way) analysis of heat budget at point S2 in Fig. 2 from initialization (12 UTC on 12 September 2004) through termination (00 UTC on 17 September 2004). Horizontal advection term in degrees Celsius per day (*upper left*), vertical advection term in degrees Celsius per day (*upper right*), total advection term in degrees Celsius per day (*middle left*), vertical diffusion term in degrees celsius per day (*middle right*), total local rate of change term in degrees Celsius per day (*lower left*), temperature in degrees Celsius (*lower right*), and comparison of contributions of advection and diffusion to local change in temperature integrated through 100 m (*bottom panel*)

model couples three state-of-the-art numerical models: WRF (atmosphere), ROMS (ocean), and SWAN (wave). The methods of model coupling, physical parameterizations, and development of initial and boundary conditions for each of the three individual numerical models were discussed.

We applied the COAWST model to hindcast Hurricane Ivan (2004); several model sensitivity experiments were conducted to examine effects of different levels of coupling among atmosphere, ocean, and wave environments. Model cases with coupling between the atmosphere, ocean, and waves demonstrate modest improvement in track but significant improvement in intensity when compared with the uncoupled cases.

For the coupled cases, ocean and wave model output were compared with in situ and remote observations. It shows that the coupled models represent the SST well, to within 1 °C, at four of the five in situ buoy stations. However, for the interior of the Gulf of Mexico on the right side of the track, both the remote and one in situ time series of observations (at buoy 42003) demonstrate

a significant model cold bias. This cold bias is likely due to the excessive mixing produced by the ocean model, a topic we will investigate and report in future research. Analyses of the heat budget illustrating the modeled effects of a strong TC interacting with the ocean are consistent with observed and theorized ocean dynamics in a hurricane environment. Likewise, coupled wave model results compare favorably to significant wave height measurement by buoys.

With the addition of wave coupling in the three-way case, treatment of the surface roughness length had a definite effect on the maximum wind speed derived in the simulations and is an area needing more study and refinement. Here, we chose to use the Taylor and Yelland (2001) scheme to calculate surface roughness length based on the significant wave height and wave period. The COAWST system provides two other parameterizations for surface roughness: that in Oost et al. (2002) and in Drennan et al. (2005). None of these sea surface roughness parameterizations are universally "best," and the choice should be made for each specific
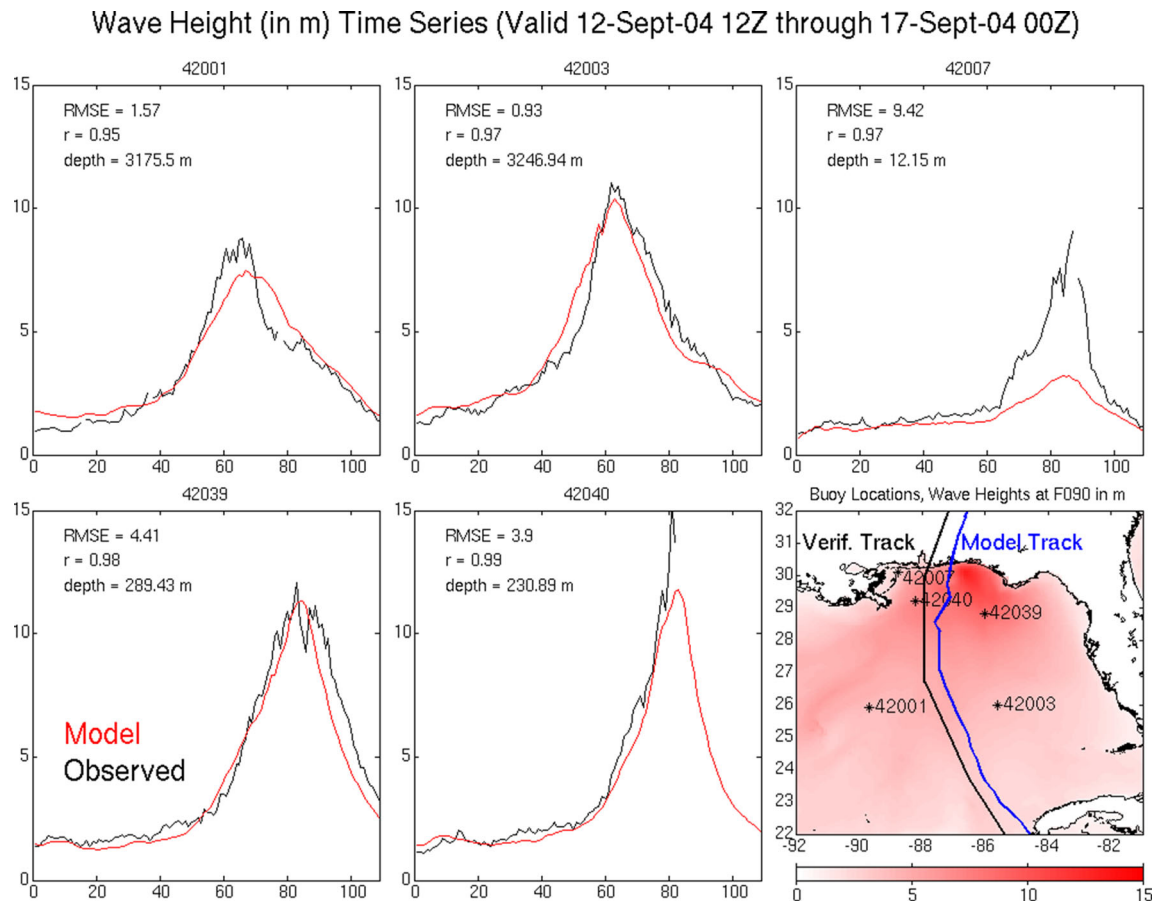
Fig. 11 Model wave comparison from initialization (12 UTC on 12 September 2004) through termination (00 UTC on 17 September 2004). Observed (*black*) and modeled (*red*) significant wave heights at five buoy locations: 42001 (*upper left*), 42003 (*upper middle*), 42007 (*upper right*), 42039 (*lower left*), and 42040 (*lower middle*). Inset (*lower right*) shows locations of buoys, simulated tracks, and wave heights at F090 (*shaded*). Some observations were not available due to extreme waves (e.g., buoy 42040 was torn from its mooring). For each comparison, the correlation coefficient and RMSE between observed and simulated significant wave heights are given, along with the water depth information of each station

case. For instance, in an examination of Hurricane Ida and Nor'easter Ida using the COAWST modeling system, Olabarrieta et al. (2012) found that the Oost sea surface parameterization (Oost et al. 2002) provided the best solution for that particular storm. Future studies examining observations and model sensitivity of different wave coupling schemes in generating the roughness length Z_0 and mixing induced by waves are clearly needed.

It is also important to note that future study of the fully coupled COAWST modeling system should include increased wave-atmosphere fluxes of latent and sensible heating caused by dissipative heating and sea spray. Bao et al. (2011) demonstrated that sea spray has a significant impact as 10-m winds climb above 30 m/s by increasing the enthalpy exchange coefficient (C_k) and reducing the 10-m neutral drag coefficient (C_D).

While a slight deviation of simulated TC track and intensity cause some difference in the comparisons to observations, the ability of the fully coupled model to resolve the atmosphere, ocean, and wave environments was shown. The use of a fully coupled model allows a detailed examination of simultaneous interactions among ocean, atmosphere, and wave environments. In a forecast situation, this model would provide very useful and comprehensive environmental conditions (of atmosphere, wave, and ocean) to agencies and emergency managers in the event of a landfalling hurricane.

Our results show that a fairly accurate 108 h simulation of the atmosphere, ocean, and wave environments can be archived without the added benefit of data assimilation, ensemble forecasting, downscaling, or other computationally expensive methods that could degrade the investigation of the dynamics within a coupled model. Future studies including these techniques may further improve the overall skill of model predictions. Contributions to the TC environment from the effects of improved drag formulations, dissipative heating, and sea spray are possible with inclusion of feedback from the wave model but are left for future study.

References

Bao JW, Wilczak JM, Choi JK (2000) Numerical simulations of air-sea interaction under high wind conditions using a coupled model: a study of hurricane development. Mon Weather Rev 128:2190–2210. doi:10.1175/1520-0493(2000)128<2190:NSOASI>2.0.CO;2

Bao JW, Fairall CW, Michelson SA, Bianco L (2011) Parameterizations of sea-spray impact on the air–sea momentum and heat fluxes. Mon Weather Rev 139:3781–3797. doi:10.1175/MWR-D-11-00007.1

Bender MA, Ginis I, Tuleya R, Thomas B, Marchok T (2007) The operational GFDL coupled hurricane–ocean prediction system and a summary of its performance. Mon Weather Rev 135:3965–3989. doi:10.1175/2007MWR2032.1

Booij N, Ris RC, Holthuijsen LH (1999) A third-generation wave model for coastal regions. Part I: model description and validation. J Geophys Res 104:7649–7666. doi:10.1029/98JC02622

Charnock H (1955) Wind stress over a water surface. Q J Roy Meteorol Soc 81:639–640

Chassignet EP, Hurlburt HE, Smedstad OM, Halliwell GR, Hogan PJ, Wallcraft AJ, Baraille R, Bleck R (2006) The HYCOM (hybrid coordinate ocean model) data assimilative system. J Mar Syst 65:60–83. doi:10.1016/j.jmarsys.2005.09.016

Chen F, Dudhia J (2001) Coupling an advanced land-surface/ hydrology model with the Penn State/NCAR MM5 modeling system. Part I: model description and implementation. Mon Weather Rev 129:569–585. doi:10.1175/1520-0493(2001)129<0569:CAALSH>2.0.CO;2

Chen SYS, Price JF, Zhao W, Donelan MA, Walsh EJ (2007) The CBLAST-hurricane program and the next-generation fully coupled atmosphere-wave-ocean. models for hurricane research and prediction. Bull Am Meteorol Soc 88:311–317. doi:10.1175/BAMS-88-3-311

Chen SS, Zhao W, Donelan MA, Tolman HL (2013) Directional wind–wave coupling in fully coupled atmosphere–wave–ocean models: results from CBLAST-hurricane. J Atmos Sci 70:3198–3215. doi:10.1175/JAS-D-12-0157.1

Davis C, Wang W, Chen SS, Chen Y, Corbosiero K, DeMaria M, Dudhia J, Holland G, Klemp J, Michalakes J, Reeves H, Rotunno R, Snyder C, Xiao Q (2008) Prediction of landfalling hurricanes with the advanced Hurricane WRF model. Mon Weather Rev 136:1990–2005. doi:10.1175/2007MWR2085.1

Done J, Davis C, Weisman M (2004) The next generation of NWP: explicit forecasts of convection using the weather research and forecast (WRF) model. Atmos Sci Lett 5:110–117. doi:10.1002/asl.72

Donelan MA, Haus BK, Reul N, Plant WJ, Stiassnie M, Graber HC, Brown OB, Saltzman ES (2004) On the limiting aerodynamic roughness of the ocean in very strong winds. Geophys Res Lett 31, L18306. doi:10.1029/2004GL019460

Doyle JD (2002) Coupled atmosphere–ocean wave simulations under high-wind conditions. Mon Weather Rev 130:3087–3099. doi:10.1175/1520-0493(2002)130<3087:CAOWSU>2.0.CO;2

Drennan WM, Taylor PK, Yelland MJ (2005) Parameterizing the sea surface roughness. J Phys Oceanogr 35:835–848. doi:10.1175/JPO2704.1

Dudhia J (1989) Numerical study of convection observed during the winter monsoon experiment using a mesoscale two-dimensional

model. J Atmos Sci 46:3077–3107. doi:10.1175/1520-0469(1989)046<3077:NSOCOD>2.0.CO;2

Fairall CW, Bradley EF, Rogers DP, Edson JB, Young GS (1996) Bulk parameterization of air-sea fluxes for tropical ocean-global atmosphere coupled-ocean atmosphere response experiment. J Geophys Res 101:3747–3764. doi:10.1029/95JC03205

Fairall CW, Bradley EF, Hare JE, Grachev AA (2003) Bulk parameterization of air-sea fluxes: updates and verification for the COARE algorithm. J Clim 16:571–591. doi:10.1175/1520-0442(2003)016<0571:BPOASF>2.0.CO;2

Fan Y, Ginis I, Hara T (2009) The effect of wind–wave–current interaction on air–sea momentum fluxes and ocean response in tropical cyclones. J Phys Oceanogr 39:1019–1034. doi:10.1175/2008JPO4066.1

Flather RA (1976) A tidal model of the northwest European continental shelf. Bull Soc Roy Sci Liege 6:141–164

Fowle MA, Roebber PJ (2003) Short-range (0–48 h) numerical prediction of convective occurrence, mode, and location. Wea Forecast 18:782–794. doi:10.1175/1520-0434(2003)018<0782:SHNPOC>2.0.CO;2

Garratt JR (1992) The atmospheric boundary layer. Cambridge University Press, Cambridge

Gemmill W, Katz B, Li X (2007) Daily real-time global sea surface temperature—high resolution analysis at NOAA/NCEP. NOAA/NWS/NCEP/MMAB Office Note 260

Goerss JS (2006) Prediction of tropical cyclone track forecast error for Hurricanes Katrina, Rita, and Wilma. Preprints, 27th Conf. on Hurricanes and Tropical Meteorology, Monterey, CA, Amer Meteor Soc 11A.1

Gopalakrishnan SG, Goldenberg S, Quirino T, Zhang X, Marks F Jr, Yeh KS, Atlas R, Tallapragada V (2012) Toward improving high-resolution numerical hurricane forecasting: influence of model horizontal grid resolution, initialization, and physics. Wea Forecast 27:647–666. doi:10.1175/WAF-D-11-00055.1

Haidvogel DB, Arango HG, Budgell WP, Cornuelle BD, Curchitser E, Di Lorenzo E, Fennel K, Geyer WR, Hermann AJ, Lanerolle L, Levin J, McWilliams JC, Miller AJ, Moore AM, Powell TM, Shchepetkin AF, Sherwood CR, Signell RP, Warner JC, Wilkin J (2008) Regional ocean forecasting in terrain-following coordinates: model formulation and skill assessment. J Comput Phys 227:3595–3624. doi:10.1016/j.jcp.2007.06.016

Halliwell GR Jr, Shay LK, Brewster JK, Teague WJ (2011) Evaluation and sensitivity analysis of an ocean model response to Hurricane Ivan. Mon Weather Rev 139:921–945. doi:10.1175/2010MWR3104.1

Hill KA, Lackmann GM (2009) Analysis of idealized tropical cyclone simulations using the weather research and forecasting model: sensitivity to turbulence parameterization and grid spacing. Mon Weather Rev 137:745–765. doi:10.1175/2008MWR2220.1

Hong SY, Lim JOJ (2006) The WRF single-moment 6-class microphysics scheme (WSM6). J Korean Meteor Soc 42:129–151

Hodur RM (1997) The naval research laboratory's coupled ocean/ atmosphere mesoscale prediction system (COAMPS). Mon Weather Rev 125:1414–1430. doi:10.1175/1520-0493(1997)125<1414:TNRLSC>2.0.CO;2

Hyun KH, He R (2010) Coastal upwelling in the South Atlantic bight: a revisit of the 2003 cold event using long term observations and model hindcast solutions. J Mar Syst 83:1–13. doi:10.1016/j.jmarsys.2010.05.014

Jacob R, Larson J, Ong E (2005) M x N communication and parallel interpolation in CCSM using the Model Coupling Toolkit. Preprints, Mathematics and Computer Science Division, Argonne National Laboratory, Argonne, IL

Jaimes B, Shay LK, Halliwell GR (2011) The response of quasigeostropic ocean vorticies to tropical cyclone forcing. Mon Weather Rev 41:1965–1985. doi:10.1175/JPO-D-11-06.1

Janjic ZI (1990) The step-mountain coordinate: physical package. Mon Weather Rev 118:1429–1443. doi:10.1175/1520-0493(1990)118<1429:TSMCPP>2.0.CO;2

Janjic ZI (1996) The surface layer in the NCEP Eta model. Extended abstracts, Eleventh Conference on Numerical Weather Prediction, Norfolk, VA, Amer Meteor Soc, 354–355

Janjic ZI (2002) Nonsingular implementation of the Mellor–Yamada Level 2.5 scheme in the NCEP Meso model. NCEP Office Note 437

Jones PW (1999) First- and second-order conservative remapping schemes for grids in spherical coordinates. Mon Weather Rev 127:2204–2210. doi:10.1175/1520-0493(1999)127<2204:FASOCR>2.0.CO;2

Kain JS (2004) The Kain–Fritsch convective parameterization: an update. J Appl Meteorol Climatol 43:170–181. doi:10.1175/1520-0450(2004)043<0170:TKCPAU>2.0.CO;2

Kirby JT, Chen TM (1989) Surface waves on vertically sheared flows: approximate dispersion relations. J Phys Oceanogr 94:1013–1027. doi:10.1029/JC094iC01p01013

Komen GJ, Hasselmann S, Hasselmann K (1984) On the existence of a fully developed wind-sea spectrum. J Phys Oceanogr 14:1271–1285. doi:10.1175/1520-0485(1984)014<1271:OTEOAF>2.0.CO;2

Kumar N, Voulgaris G, Warner JC, Olabarrieta M (2012) Implementation of the vortex force formalism in the coupled ocean–atmosphere–wave–sediment transport (COAWST) modeling system for inner shelf and surf zone applications. Ocean Model 47:65–95. doi:10.1016/j.ocemod.2012.01.003

Kurihara Y, Bender MA, Ross RJ (1993) An initialization scheme of hurricane models by vortex specification. Mon Weather Rev 121:2030–2045. doi:10.1175/1520-0493(1993)121<2030:AISOHM>2.0.CO;2

Kurihara Y, Bender MA, Tuleya RE, Ross RJ (1995) Improvements in the GFDL hurricane prediction system. Mon Weather Rev 123:2791–2801. doi:10.1175/1520-0493(1995)123<2791:IITGHP>2.0.CO;2

Larson J, Jacob R, Ong E (2004) The model coupling toolkit: a new Fortran90 toolkit for building multiphysics parallel coupled models. Preprints, Mathematics and Computer Science Division, Argonne National Laboratory, Argonne, IL

Lee C-Y, Chen SS (2014) Stable boundary layer and its impact on tropical cyclone structure in a coupled atmosphere–ocean model. Mon Weather Rev 142:1927–1944. doi:10.1175/MWR-D-13-00122.1

Lee C-Y, Chen SS (2012) Symmetric and asymmetric structures of hurricane boundary layer in coupled atmosphere–wave–ocean models and observations. J Atmos Sci 69:3576–3594. doi:10.1175/JAS-D-12-046.1

Leipper DF, Volgenau D (1972) Hurricane heat potential of the Gulf of Mexico. J Phys Oceanogr 2:218–224. doi:10.1175/1520-0485(1972)002<0218:HHPOTG>2.0.CO;2

Liu B, Liu H, Xie L, Guan C, Zhao D (2011) A coupled atmosphere–wave–ocean modeling system: simulation of the intensity of an idealized tropical cyclone. Mon Weather Rev 139:132–152. doi:10.1175/2010MWR3396.1

Liu L, Fei J, Cheng X, Huang X (2012) Effect of wind–current interaction on ocean response during Typhoon Kaemi (2006). Sci China Earth Sci 56:418–433. doi:10.1007/s11430-012-4548-3

Ma Z, Fei J, Liu L, Huang X, Cheng X (2013) Effects of the cold core eddy on tropical cyclone intensity and structure under idealized air–sea interaction conditions. Mon Weather Rev 141:1285–1303. doi:10.1175/MWR-D-12-00123.1

Madsen OS, Poon YK, Graber HC (1988) Spectral wave attenuation by bottom friction: theory. In: Proc 21th Int Conf Coastal Engineering, Torremolinos, Spain, Am Soc Civ Eng 492–504

Marks FD, Shay LK (1998) Landfalling tropical cyclones: forecast problems and associated research opportunities. Bull Am Meteorol Soc 79:305–323

Marchesiello P, McWilliams JC, Shchepetkin AF (2001) Open boundary conditions for long-term integration of regional oceanic models. Ocean Model 3:1–20. doi:10.1016/S1463-5003(00)00013-5

Mellor GL, Yamada T (1982) Development of a turbulence closure model for geophysical fluid problems. Rev Geophys Space Phys 20:851–875. doi:10.1029/RG020i004p00851

Mlawer EJ, Taubman SJ, Brown PD, Iacono MJ, Clough SA (1997) Radiative transfer for inhomogeneous atmosphere: RRTM, a validated correlated-k model for the longwave. J Geophys Res 102:16663–16682. doi:10.1029/97JD00237

Monin AS, Obukhov AM (1954) Basic laws of turbulent mixing in the surface layer of the atmosphere. Contrib Geophys Inst Acad Sci 151:163–187

Moon IJ, Ginis I, Hara T, Thomas B (2007) A physics-based parameterization of air–sea momentum flux at high wind speeds and its impact on hurricane intensity predictions. Mon Weather Rev 135:2869–2878. doi:10.1175/MWR3432.1

Nelson J, He R (2012) Effect of the Gulf stream on winter extratropical cyclone outbreaks. Atmos Sci Lett 13:311–316. doi:10.1002/asl.400

Oey LY, Ezer T, Wang DP, Yin XQ, Fan SJ (2006) Loop current warming by Hurricane Wilma. Geophys Res Lett 33, L08613. doi:10.1029/2006GL025873

Olabarrieta M, Warner JC, Kumar N (2011) Wave–current interaction in Willapa Bay. J Geophys Res 116, C12014. doi:10.1029/2011JC007387

Olabarrieta M, Warner JC, Armstrong B, He R, Zambon JB (2012) Ocean–atmosphere dynamics during Hurricane Ida and Nor'Ida: an application of the coupled ocean–atmosphere–wave–sediment transport (COAWST) modeling system. Ocean Model 43–44:112–137. doi:10.1029/2011JC007387

Oost WA, Komen GJ, Jacobs CMJ, van Oort C (2002) New evidence for a relation between wind stress and wave age from measurements during ASGAMAGE. Bound Layer Meteor 103:409–438

Prasad TG, Hogan PJ (2007) Upper-ocean response to Hurricane Ivan in a 1/25° nested Gulf of Mexico HYCOM. J Geophys Res 112, C04013. doi:10.1029/2006JC003695

Price JF (1981) Upper ocean response to a hurricane. J Phys Oceanogr 11:153–175. doi:10.1175/1520-0485(1981)011<0153:UORTAH>2.0.CO;2

Price JF, Sanford TB, Forristall GZ (1994) Forced stage response to a moving hurricane. J Phys Oceanogr 24:233–260. doi:10.1175/1520-0485(1994)024<0233:FSRTAM>2.0.CO;2

Pollard RT, Rhines PB, Thompson RORY (1973) The deepening of the wind-mixed layer. Geophys Astrophys Fluid Dyn 3:381–404. doi:10.1080/03091927208236105

Powell MD, Houston SH, Amat LR, Morisseau-Leroy N (1998) The HRD real-time hurricane wind analysis system. J Wind Eng Ind Aerodyn 77–78:53–64. doi:10.1016/S0167-6105(98)00131-7

Rogers R, Aberson S, Black M, Black P, Cione J, Dodge P, Gamache J, Kaplan J, Powell M, Dunion J, Uhlhorn E, Shay N, Surgi N (2006) The intensity forecasting experiment: a NOAA multiyear field program for improving tropical cyclone intensity forecasts. Bull Am Meteorol Soc 87:1523–1537. doi:10.1175/BAMS-87-11-1523

Shay LK, Ali MM, Barbary D, D'Asaro EA, Halliwell G, Doyle J, Fairall C, Ginis I, Lin II, Moon IJ, Sandery P, Uhlhorn E, Wada A (2010) Air–sea interface and oceanic influences. In: 7th WMO International Workshop on Tropical Cyclones (IWTC-VII), St. Gilles Les Bains, La Réunion, France, World Meteor Org. http://www.wmo.int/pages/prog/arep/wwrp/tmr/otherfileformats/documents/1_3.pdf. Accessed 29 August 2013

Shchepetkin AF, McWilliams JC (2005) The regional ocean modeling system: a split-explicit, free-surface, topography-following coordinates ocean model. Ocean Model 9:347–404. doi:10.1016/j.ocemod.2004.08.002

Skamarock WC, Klemp JB, Dudhia J, Gill DO, Barker DM, Wang W, Powers JG (2005) A description of the advanced research WRF version 2. NCAR Technical Note

Stewart S (2005) Tropical cyclone report: Hurricane Ivan 2–24 September 2004. National Hurricane Center. http://www.nhc.noaa.gov/2004ivan.shtml. Accessed 17 June 2013

Taylor PK, Yelland MJ (2001) The dependence of sea surface roughness on the height and steepness of the waves. J Phys Oceanogr 31:572–590. doi:10.1175/1520-0485(2001) 031<0572:TDOSSR>2.0.CO;2

Teague WJ, Jarosz E, Wang DW, Mitchell DA (2007) Observed oceanic response over the upper continental slope and outer shelf during Hurricane Ivan. J Phys Oceanogr 37:2181–2206. doi:10.1175/JPO3115.1

Wada A, Cronin MF, Sutton AJ et al (2013a) Numerical simulations of oceanic pCO_2 variations and interactions between Typhoon Choi-wan (0914) and the ocean. J Geophys Res Oceans 118:2667–2684. doi:10.1002/jgrc.20203

Wada A, Kohno N, Kawai Y (2010) Impact of wave–ocean interaction on Typhoon Hai-Tang in 2005. SOLA 6A:13–16. doi:10.2151/sola.6A-004

Wada A, Uehara T, Ishizaki S (2014) Typhoon-induced sea surface cooling during the 2011 and 2012 typhoon seasons: observational evidence and numerical investigations of the sea surface cooling effect using typhoon simulations. Prog Earth Planet Sci 64:3562–3578. doi:10.1175/JAS4051.1

Wada A, Usui N, Kunii M (2013b) Interactions between typhoon Choi-wan (2009) and the Kuroshio extension system. Adv Meteorol 2013:1–17. doi:10.5670/oceanog.2011.91

Wang Y, Wu CC (2004) Current understanding of tropical cyclone structure and intensity changes—a review. Meteorol Atmos Phys 87:257–278. doi:10.1007/s00703-003-0055-6

Walker ND, Leben RR, Balasubramanian S (2005) Hurricane-forced upwelling and chlorophyll a enhancement within cold-core cyclones in the Gulf of Mexico. Geophys Res Lett 32, L18610. doi:10.1029/2005GL023716

Warner JC, Perlin N, Skyllingstad E (2008) Using the model coupling toolkit to couple earth system models. Environ Model Softw 23: 1240–1249

Warner JC, Armstrong B, He R, Zambon JB (2010) Development of a coupled ocean–atmosphere–wave–sediment transport (COAWST) modeling system. Ocean Model 35:230–244. doi:10.1016/j.oceanmod.2010.07.010

Wu CC, Lee CY, Lin II (2007) The effect of the ocean eddy on tropical cyclone intensity. J Atmos Sci 64:3562–3578. doi:10.1175/JAS4051.1

Yablonsky RM, Ginis I (2009) Limitation of one-dimensional ocean models for coupled hurricane–ocean model forecasts. Mon Weather Rev 137:4410–4419. doi:10.1175/2009MWR2863.1

Yablonsky RM, Ginis I (2013) Impact of a warm ocean eddy's circulation on hurricane-induced sea surface cooling with implications for hurricane intensity. Mon Weather Rev 141:997–1021. doi:10.1175/MWR-D-12-00248.1